ELSEVIER

Ceramics International 30 (2004) 2203–2209

CERAMICS INTERNATIONAL

www.elsevier.com/locate/ceramint

Influence of α-Al_2O_3 addition on sintering and grain growth behaviour of 8 mol% Y_2O_3-stabilised cubic zirconia (c-ZrO_2)

S. Tekeli*, M. Erdogan, B. Aktas

Materials Division, Metallurgy Education Department, Faculty of Technical Education, Gazi University, 06500 Besevler-Ankara, Turkey

Received 20 November 2003; received in revised form 1 December 2003; accepted 28 January 2004
Available online 20 April 2004

Abstract

The effect of α-Al_2O_3 addition on sintering and grain growth behaviour of high purity 8 mol% yttria-stabilised cubic zirconia (c-ZrO_2) was investigated. For these purposes, 1 wt.% α-Al_2O_3 was selected as a dopant in c-ZrO_2. The slip-cast specimens were sintered at different temperatures between 1150 and 1400 °C. It was seen that doped c-ZrO_2 had a faster sintering rate and lower sintering temperature than undoped c-ZrO_2. In particular, doped c-ZrO_2 achieved a density of 95% of its theoretical value at 1275 °C, while undoped c-ZrO_2 reached the same value at 1325 °C. The different sinterability of doped c-ZrO_2 and undoped c-ZrO_2 can be attributed to their different behaviour of grain growth. For grain growth measurements, the specimens sintered at 1400 °C were annealed at 1400, 1500 and 1600 °C for 10, 30 and 66 h. It was seen that grain growth rate could be controlled by the deliberate addition of 1 wt.% grain boundary phase of α-Al_2O_3. A grain growth exponent of 2 and activation energy for grain growth of 298 kJ/mol were obtained for undoped c-ZrO_2. The α-Al_2O_3 containing specimens had a grain growth exponent of 3 and activation energy of 361 kJ/mol. The slow grain growth in doped c-ZrO_2 is attributed to solute ions segregation in grain boundary region. The addition of the grain boundary phase results in limiting matter transfer along the grain boundary resulting in slower grain growth.

Keywords: A. Grain growth; Cubic zirconia; Sinterability

1. Introduction

Zirconia ceramics consist of three polymorphs; monoclinic, tetragonal and cubic. These phases can be obtained depending on temperature and compositional ranges under equilibrium conditions [1–3]. Monoclinic zirconia is present below 1240 °C and is the stable room temperature phase of pure zirconia. Tetragonal zirconia is an intermediate phase, which lies between 1240 and 2370 °C. The retention of the tetragonal phase can be controlled as in the case of cubic zirconia by the addition of dopants. Y_2O_3 additions yield an extremely fine grained microstructure known as tetragonal zirconia polycrystal which has excellent mechanical properties. Cubic zirconia is the highest temperature phase which is present in the temperature range of 2370 and 2680 °C. However, upon the addition of a few percent of stabilisers; such as CaO, MgO or Y_2O_3, the cubic phase can be obtained at lower temperatures [1,2]. The high-temperature cubic phase can also be retained at room temperatures as a non-equilibrium phase by rapid cooling such that diffusive transformation does not occur. The cubic form of stabilised zirconia ceramics are of technological importance due to their high oxygen ionic conductivity at around 1000 °C. Their use as solid state electrolytes has allowed the creation of novel application such as oxygen gas sensors, oxygen membrane separators and solid oxide fuel cells (SOFCs).

High-temperature deformation in fine-grained ceramics has been extensively studied in recent years. Large tensile elongations have been found in many ceramics and ceramic composites such as yttria-stabilised zirconia [4,5], alumina [6,7], hydroxyapatite [8], zirconia–alumina [9,10], mullite–zirconia [11], silicon carbide [12], silicon nitride–silicon carbide [13,14] and iron–iron carbide [15]. Of the above materials, tetragonal zirconia has been intensively investigated, beginning with the work of Wakai et al. [4], in which a tensile elongation to failure of 100% at 1723 K was obtained. In the ensuing years, tensile ductility in the same material has been improved and Kajihara

* Corresponding author. Tel.: +90-312-4399760; fax: +90-312-2120059.
E-mail address: stekeli@gazi.edu.tr (S. Tekeli).

0272-8842/$30.00 © 2004 Elsevier Ltd and Techna S.r.l. All rights reserved.
doi:10.1016/j.ceramint.2004.01.004

et al. [16] have reported an elongation to failure of 1038% in 2.5Y-TZP containing 5 wt.% SiO_2 at 1673 K and at $1.3 \times 10^{-4}\,s^{-1}$. In contrast, such elongations have not been obtained in cubic zirconia despite attempts to attain the high-temperature ductility. As stated by Chen and Xue [17] microstructural superplasticity requires an ultra fine grain size that is stable against coarsening during sintering and high-temperature deformation. A low sintering temperature is a necessary, but not a sufficient condition for achieving the required microstructure. In many cases, it seems that the selection of an appropriate crystalline phase is also crucial for obtaining an ultra fine grain size; for instance, tetragonal zirconia is superplastic whereas cubic zirconia is not. Extensive ductilities in tetragonal zirconia are a consequence of grain size stability during sintering and high-temperature deformation. Compared to tetragonal zirconia, cubic zirconia suffers fast grain growth and shows almost no ductility.

The present study was, therefore, undertaken with the aim of investigating the effect of α-Al_2O_3 addition on sintering and grain growth behaviour of high purity 8 mol% yttria-stabilised cubic zirconia (c-ZrO_2).

2. Experimental: materials and procedures

The materials used in the present work were 8 mol% yttria-stabilised cubic zirconia (c-ZrO_2) powder and high purity (>99.999%) α-Al_2O_3 powder, supplied by Mandoval Ltd., Zirconia Sales (UK) Ltd. The average particle sizes were 0.3 μm for c-ZrO_2 and 0.4 μm for α-Al_2O_3. The chemical composition of the powders provided from the manufactures is listed in Table 1.

A slip-casting method was used for the preparation of specimens for density, grain growth, phase content and lattice parameter measurements. Slip-casting allowed homogeneous dispersion of powders and the economical production of net shapes that required no machining. The slip-casting slurry was prepared by dispersing the designated amount of the powders (c-ZrO_2 and α-Al_2O_3) in distilled water with a dispersing agent (Dispex A40); the slurry was then wet ball milled for 4 h to obtain a good dispersion and to break-up agglomerates in a plastic container using zirconia balls. The milled slurry was injected by a syringe into a plaster mould. Cast specimens were released from the mould after ∼60 min and then air-dried at ∼25 °C for a few days. The green density of slip-cast specimens was between 45 and 50% of the theoretical density. These specimens were presintered at 950 °C to make them more handleable and smooth surfaces were obtained by carefully grinding off any casting protrusions. For density and grain growth measurements, c-ZrO_2 specimens containing 1 wt.% Al_2O_3 were used. For the determination of phase content and lattice parameter, specimens containing Al_2O_3 dopant in amounts up to 5 wt.% were used. The green density of the slip-cast specimens was measured from the volume and weight.

To determine optimal sintering temperature, the specimens were sintered at different temperatures between 1150 and 1400 °C in air at a constant heating rate of 200 °C/h for 1 h. The density of sintered specimens was determined by the Archimedes method.

The specimens for grain growth measurements were first sintered at 1350 °C for 1 h before annealing. Grain growth was examined by annealing sintered specimens for 10, 30 and 66 h at temperatures between 1400 and 1600 °C. After annealing, the specimens were sectioned, ground, polished to 1 μm surface finish and finally thermally etched in air for 30 min at a temperature 50 °C lower than annealing temperature. Scanning electron microscopy (SEM) equipped with an energy dispersive X-ray spectrometer (EDS) attachment was used to characterise the microstructure of as-sintered and annealed specimens. Grain sizes were measured by the mean linear intercept method. An average grain size was obtained by multiplying 1.78 to average intercept lengths over 1000 grains. Phase determination and unit cell lattice parameters were determined using XRD (2θ: 20–60°, scan speed: 0.1).

3. Experimental results and discussion

X-ray diffraction measurements were carried out on specimens containing Al_2O_3 dopant in amounts up to 5 wt.%. X-ray diffraction data showed that all specimens contained only cubic fluorite structure. Fig. 1 shows the variation of the average lattice parameter of the cubic lattice with dopant amount. As can be seen from this figure, the average lattice parameter varied linearly with the amount of Al_2O_3 dopant up to 0.3 wt.% and then levelled off. The lower values of the lattice parameter found for doped c-ZrO_2 could be due to the dissolution in the cubic phase of some Al_2O_3 which has a smaller ionic radius than Zr^{4+} and Y^{3+} and thus replacing the smaller Al^{3+} ions with Zr^{4+} and Y^{3+} in the cubic lattice (the ionic radius of Al^{3+}, Y^{3+} and Zr^{4+} are 0.54, 1.015 and 0.84, respectively). Decrease in unit cell size from

Table 1
Chemical composition of the powders

Materials	Composition (wt.%)							
	ZrO_2 (+HfO_2)	Y_2O_3	Al_2O_3	SiO_2	TiO_2	Fe_2O_3	Na_2O	CaO
c-ZrO_2	85.9	13.6	0.25	0.1	0.10	0.003	0.01	0.02
α-Al_2O_3	–	–	99.9	0.04–0.08	–	0.01–0.02	0.08	–

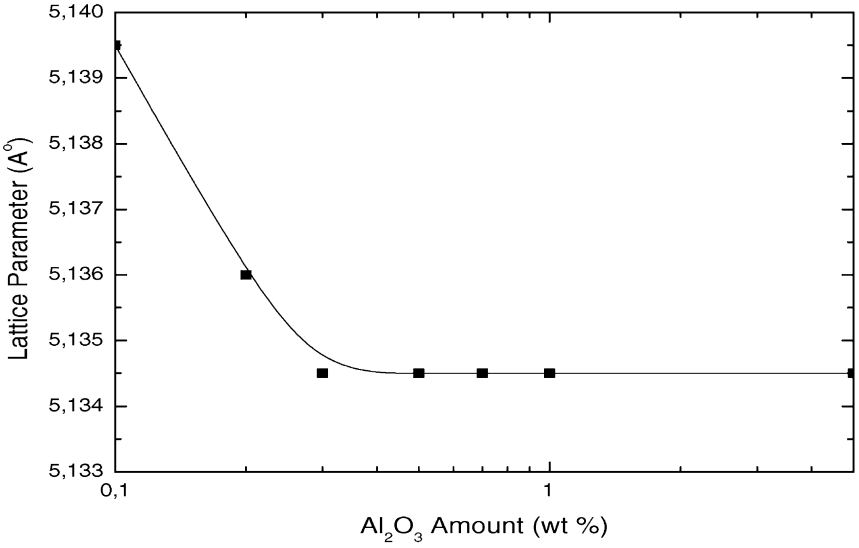

Fig. 1. Variation of lattice parameter with Al_2O_3 dopant amount.

5.139 to 5.134 Å indicated that around 0.3 wt.% Al_2O_3 had dissolved into the cubic fluorite structure. As the solubility limit of Al_2O_3 in c-ZrO_2 is ~0.3 wt.%, Al_2O_3 can hardly form a solid solution with c-ZrO_2. Therefore, Al_2O_3 mostly segregates around the c-ZrO_2 particles and at grain boundaries. There are two factors which may contribute to the segregation of ions at the grain boundaries of oxide ceramics [18,19]. One is the strain energy relaxation that results from the size mismatch between the solute and host ions, and the other is electrostatic charge compensation. The size mismatch can be approximated in terms of misfit value Σ as follows:

$$\Sigma = \frac{r_1 - r_2}{r_1} \quad (1)$$

where r_1 and r_2 are the ionic radii of solvent and solute ions. The strain energy relaxation is the principal driving force for the segregation, when the misfit value is large. It is found that the misfit value of Al^{3+} is 0.36 and a large driving force for segregation at grain boundaries, instead of forming solid solution in matrix, is expected for trivalent Al^{3+} because of the considerable size mismatch and the charge difference between Al^{3+} and Zr^{4+}.

Generally, an acceptable relative density of c-ZrO_2 electrolyte for solid oxide fuel cells has been reported to be >94% [20]. It was found that densities greater than 95% of the theoretical value could easily be achieved by pressureless sintering. After sintering, it was seen that the dimensions of the sintered specimens varied with composition due mainly to differences in green densities. Fig. 2 shows the relative density of c-ZrO_2 without Al_2O_3 and with Al_2O_3 as a function of sintering temperature. The relative densities of the specimens increased with elevating the sintering temperature. It was seen that doped c-ZrO_2 had a faster sintering rate and

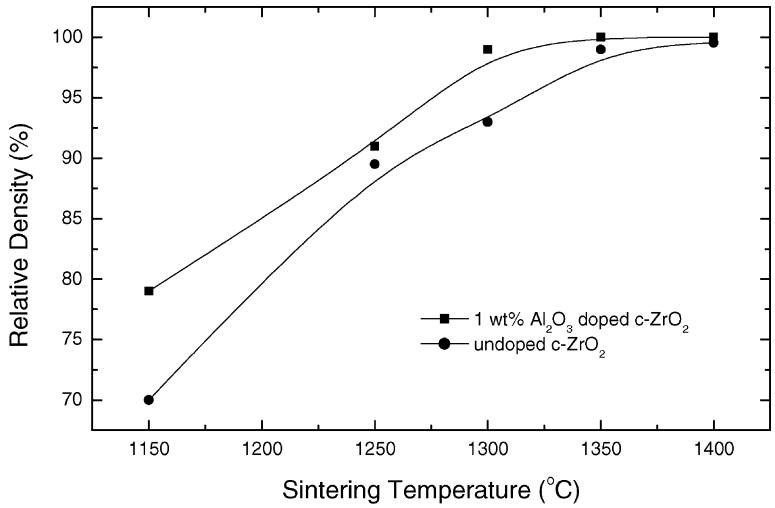

Fig. 2. Relative density vs. sintering temperature.

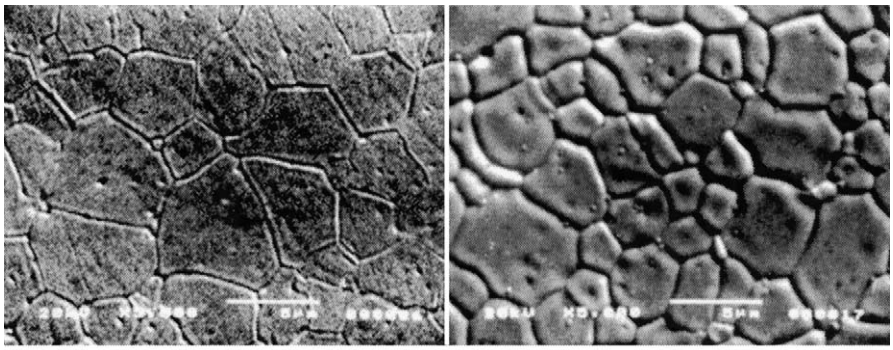

Fig. 3. Microstructures of polished and thermally-etched specimens sintered at 1400 °C for 1 h before annealing: (a) undoped c-ZrO_2 and (b) 1 wt.% Al_2O_3 doped c-ZrO_2.

lower sintering temperature than undoped c-ZrO_2. In particular, doped c-ZrO_2 achieved a density of 95% of its theoretical value at 1275 °C, while undoped c-ZrO_2 reached the same value at 1325 °C. The different sinterebility of doped c-ZrO_2 and undoped c-ZrO_2 can be attributed to their different behaviour of grain growth. In order to achieve full densification, excessive grain growth has to be inhibited either by incorporation of the second phase particle or solid solution

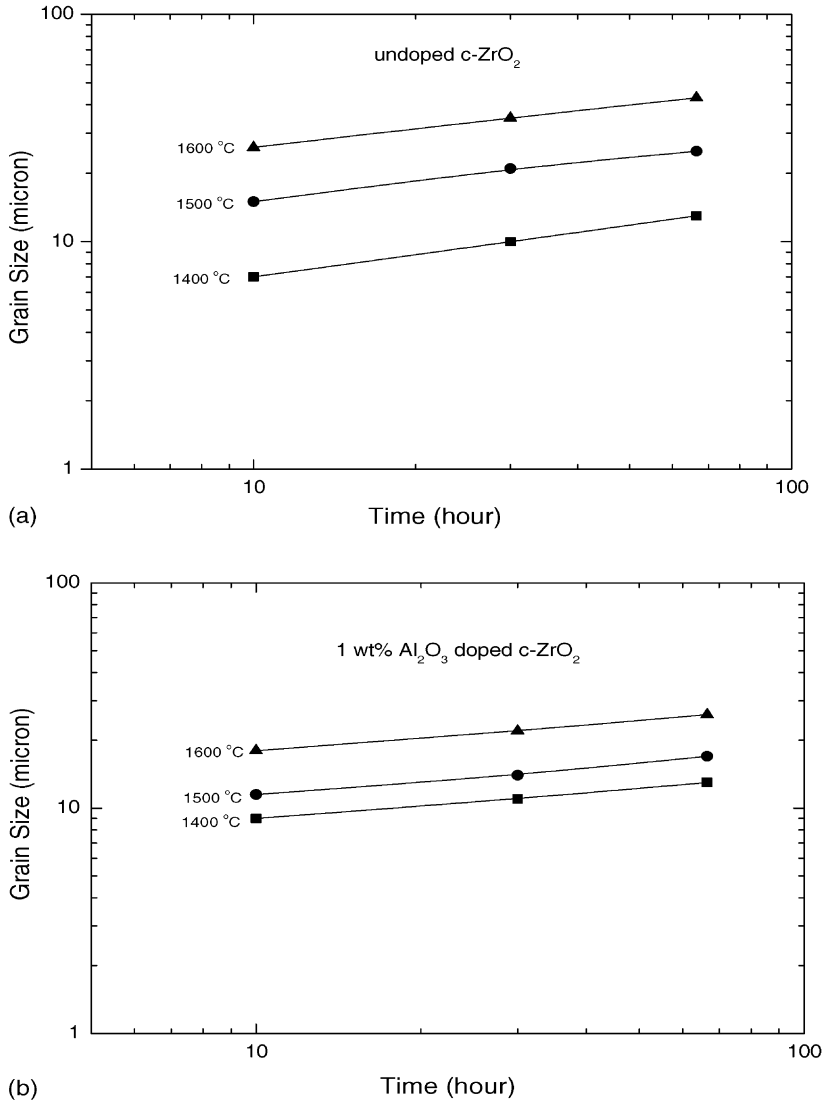

Fig. 4. Grain size as a function of annealing time for: (a) undoped c-ZrO_2 and (b) doped c-ZrO_2.

alloying during sintering and high-temperature deformation. The decreased density in undoped c-ZrO_2 is quite evident. Examination of the sintered microstructures revealed large cubic grains containing intragranular pores. Thus, the role of grain growth in sintering of cubic zirconia ceramic appears to be a classical one: a faster grain growth causes pore detachment from grain boundaries, preventing full densification at lower temperatures [21]. In polycrystalline materials, particles of a second phase with limited solubility are most effective in pinning grain boundaries and thus in minimising grain growth. The presence of the alumina in zirconia enhance the stability of material. Therefore, the extensive grain coarsening as observed in the single ceramics was not observed.

Fig. 3 is the microstructures of undoped c-ZrO_2 and doped c-ZrO_2 sintered at 1400 °C for 1 h prior to annealing. The comparison of the grain size of the two alloys at the same heat treatment indicates that grains are larger in undoped c-ZrO_2 than in doped c-ZrO_2. The grains were regular in shape and the pores were mainly at grain boundaries. Grain growth during high-temperature annealing was investigated in undoped c-ZrO_2 and doped c-ZrO_2 between 1400 and 1600 °C for 10, 30 and 66 h. The grain growth exponent, n, is obtained by plotting $\ln D$ versus $\ln t$ as shown in Fig. 4a and b. It is evident that in both ceramics, grains became larger during high-temperature annealing and the extent of grain growth increased with increase in annealing temperature and time. Also it can be seen from Fig. 4a and b that grain growth rates could be controlled by the deliberate addition of 1 wt.% grain boundary phase of α-Al_2O_3. Grain growth exponent values obtained during these tests were 2 for undoped c-ZrO_2 and 3 for doped c-ZrO_2. Representative microstructures of undoped c-ZrO_2 and doped c-ZrO_2 annealed at 1400 °C for 10, 30 and 66 h in air are shown in Fig. 5.

The kinetics of grain growth are deduced by analysing the grain size as a function of annealing time in accordance with the classical theory for grain growth [22]:

$$D^n - D_o^n = k(t - t_o) \tag{2}$$

$$k = k_o \exp\left(\frac{-Q}{RT}\right) \tag{3}$$

where D is the grain size at time t; D_o, reference grain size at time t_o; n, constant for a given grain growth mechanism;

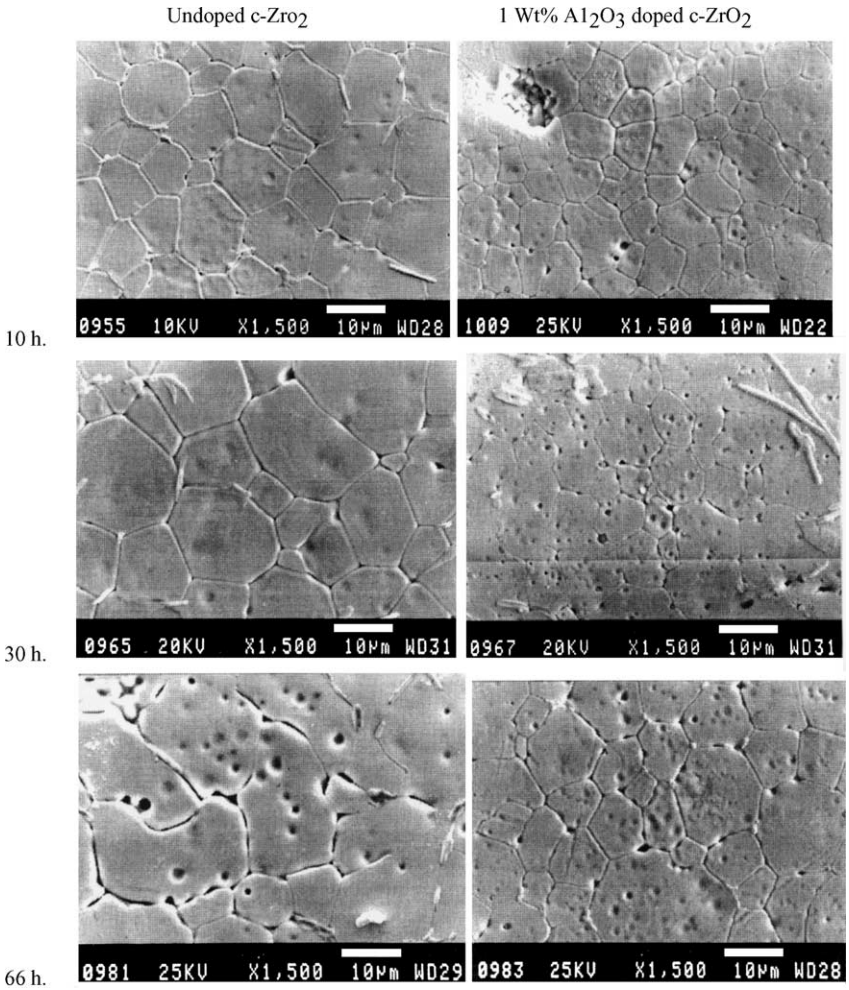

Fig. 5. SEM micrographs of undoped c-ZrO_2 and doped c-ZrO_2. These specimens were annealed at 1400 °C for 10, 30 and 66 h.

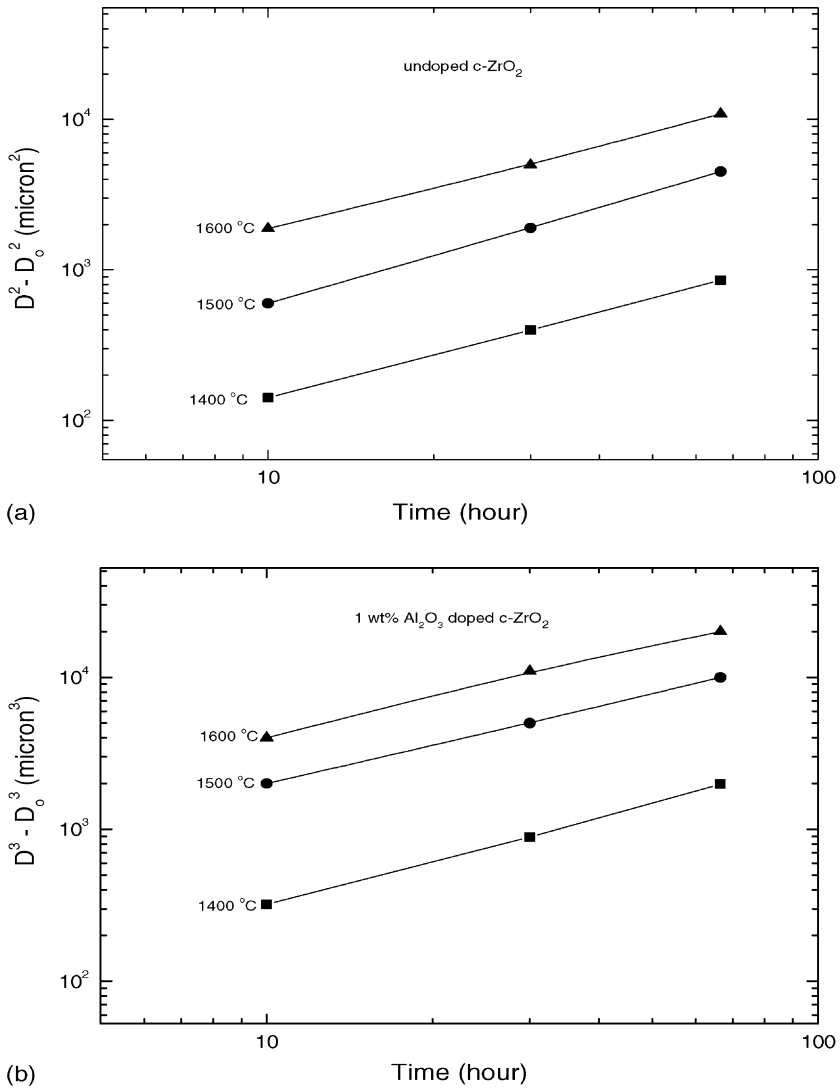

Fig. 6. The relationship between grain size difference and annealing time for (a) undoped c-ZrO_2 and (b) doped c-ZrO_2.

k, temperature-dependent constant; k_0, temperature insensitive constant and Q, R and T are activation energy, gas constant and absolute temperature, respectively. A value of $n = 2$ suggest normal grain growth. A value of $n = 3$ indicates a solid solution drag-controlled grain growth.

In Fig. 6a and b, the data points fall on straight lines, and the kinetic constant, k, which is the slope in Fig. 4a and b, is greater for undoped c-ZrO_2 than it is for doped c-ZrO_2. In other words, the grain growth in undoped c-ZrO_2 is faster than in doped c-ZrO_2. To evaluate the activation energy for grain growth, the kinetic constant k is plotted as a function of the reciprocal of the absolute temperature (Fig. 7). It can be seen from this figure that, the activation energy, Q, for doped c-ZrO_2 is higher than that for undoped c-ZrO_2. The activation energy values are approximately 289 and 361 for undoped c-ZrO_2 and for doped c-ZrO_2, respectively. This increase in activation energy is accompanied by a decrease in grain size.

In order to reduce or suppress the grain growth the grain boundary mobility and energy can be reduced for example by impurities, pores, dopants or particles of a second phase. In polycrystalline materials, it has been shown that particles of a second phase with limited solubility are especially effective in pinning grain boundaries and thus in minimising static and dynamic grain growth [23]. As stated by Sturm et al. [24] in order to provide efficient grain boundary pinning in a nanocrystalline structure the particles of the second phase have to fulfil several of the following conditions: (a) small diffusion coefficient of the solute cations into the matrix, (b) small or no solubility of the solute cations in the matrix, (c) a small interfacial energy between the two phases, (d) a homogeneous distribution of the second phase and (e) stability against dissolution and coarsening.

The differences in grain growth in undoped c-ZrO_2 and doped c-ZrO_2 can be related to differences in segregation of the solute cations at grain boundaries. SEM with EDS analysis showed that the concentration of Al_2O_3 dopant near the

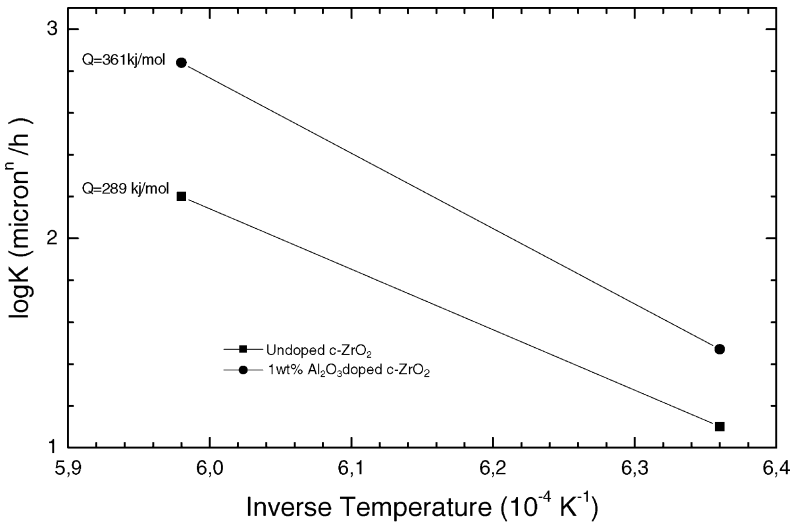

Fig. 7. Grain growth constant, *k*, as a function of the reciprocal absolute temperature.

grain boundary region in doped c-ZrO_2 was higher than in undoped c-ZrO_2. In the light of the above results it is deduced that the grain size stability is associated with segregation of solute cation to grain boundaries, which lowers grain boundary mobility and grain boundary energy, thus increasing the cohesive strength of the grain boundary and the diffusion distance across the boundary. Low solubility of Al_2O_3 acts as a barrier against diffusion. Due to the lower solubility of Al_2O_3 in c-ZrO_2, grain growth is expected to be slower in Al_2O_3 containing specimens. Compared to doped c-ZrO_2, undoped c-ZrO_2 suffers fast grain growth and only limited cation segregation to grain boundaries; consequently, undoped c-ZrO_2 has a lower grain boundary cohesive strength and a higher grain boundary mobility and energy.

4. Conclusions

Grain growth in doped c-ZrO_2 occurs slowly and is more sluggish than that in undoped c-ZrO_2. This is mainly due to the lower grain boundary mobility and energy which results from solute segregation in the grain boundary and its drag in doped c-ZrO_2 but not in undoped c-ZrO_2. The drag effect arises from any preferred segregation of an impurity either to or from grain boundary area because of size and charge differences. Al_2O_3 addition is expected to segregate to grain boundaries. This segregation layer is believed to hinder grain growth by resulting in limiting matter transfer along the grain boundary.

Acknowledgements

One of the authors (S. Tekeli) thanks TÜBiTAK (the Science and Technology Research Council of Turkey) for providing financial support under BAYG-C program for this work.

References

[1] C.F. Grain, J. Am. Ceram. Soc. 50 (6) (1967) 288.
[2] H.G. Scott, J. Mater. Sci. 10 (9) (1975) 1527.
[3] S. Kazutaka, Ph.D. thesis, Tokyo University, 2001.
[4] F. Wakai, S. Sakaguchi, Y. Matsuna, Adv. Ceram. Mater. 1 (3) (1986) 259.
[5] F. Wakai, S. Sakaguchi, K. Kanayama, H. Kato, H. Onishi, Ceramic Materials and Components for Engines, Deutsehe Keramische Gesellschaft Bad, Honnet, 1986, p. 315.
[6] W.R. Canon, W.H. Rhodes, A.H. Heuer, J. Am. Ceram. Soc. 63 (1980) 46–53.
[7] Z.C. Wang, T.J. Davies, N. Ridley, A.A. Ogwu, Acta Mater. 11 (1996) 4301–4309.
[8] F. Wakai, Y. Kodama, S. Sakaguchi, T. Nonami, J. Am. Ceram. Soc. 73 (1990) 257.
[9] F. Wakai, H. Kato, Adv. Ceram. Mater. 3 (1988) 71.
[10] T.G. Nieh, C.M. McNally, J. Wadsworth, Scripta Metall. 23 (1987) 457.
[11] C.K. Yoon, W.I. Chen, J. Am. Ceram. Soc. 73 (1990) 1555.
[12] C. Carry, A. Mocellin, Deformation of Ceramics II, Plenum Press, New York, 1984, p. 391.
[13] F. Wakai, Y. Kodama, S. Sakaguchi, K. Murayama, K. Izaki, K. Niihara, Nature 344 (1990) 421.
[14] T. Rouxel, F. Wakai, K. Izaki, J. Am. Ceram. Soc. 75 (1992) 2363.
[15] W.J. Kim, J. Wolfenstine, G. Frommeyer, O.D. Sherby, Scripta Metall. 23 (1989) 1515.
[16] K. Kajihara, Y. Yoshizawa, T. Sakuma, Scripta Metall. 28 (1993) 559–562.
[17] I.W. Chen, L.A. Xue, J. Am. Ceram. Soc. 73 (9) (1990) 2585–2609.
[18] A.J. Burggraaf, A.J. Winnubst, in: J. Nowotny, L.C. Dufour (Eds.), Surface and Near-Surface Chemistry of Oxide Materials, Elsevier, Amsterdam, 1988, pp. 449–474.
[19] Y. Ikuhara, T. Yamamoto, A. Kuwabara, H.T. Sakuma, Sci. Technol. Adv. Mater. 2 (2001) 411–424.
[20] M. Mori, M. Yoshikawa, H. Itoh, T. Abe, J. Am. Ceram. Soc. 8 (1994) 2217–2219.
[21] I.G. Lee, I. Wei Chen, in: S. Somya, M. Shinada, M. Yoshimua, R. Watanabe (Eds.), Sintering 87, Elsevier, UK, 1988, pp. 340–345.
[22] R.J. Brook, in: Treatise on Materials Science and Technology, Academic Press, New York, 1976.
[23] I.-W. Chen, L.A. Xue, J. Am. Ceram. Soc. 73 (1990) 2585.
[24] A. Sturm, U. Betz, G. Scipione, H. Hahn, NanoStruct. Mater. 11 (5) (1999) 651–661.